

# Field-Induced Ferroelectric Phase Transition Dynamics in PMN-PT compositions near the Morphotropic Phase Boundary

Shivjeet Chanan,<sup>1</sup> Joseph A. Kerchenfaut,<sup>1</sup> Eduard Ilin,<sup>1</sup> and Eugene V. Colla<sup>1,\*</sup>

<sup>1</sup>*Department of Physics, University of Illinois at Urbana-Champaign, 1110 W Green St Urbana IL 61801-3080, USA*

(Dated: January 30, 2026)

The dynamical behavior of field-induced ferroelectric phase transitions in compositions of  $\text{PbMg}_{1/3}\text{Nb}_{2/3}\text{O}_3(1-x)\text{-PbTiO}_3(x)$ , called PMN-PT, near the Morphotropic Phase Boundary (MPB) was investigated through several different external electrical field application protocols. Our results indicate that the phase transitions in PMN-PT compositions near the MPB behave differently than in compositions far below the MPB. We show that the electrical-field history has a notable impact on the field-induced transition temperature  $T_c$ , ZFC delay time  $\tau_{ZFC}$ , and induced polarization  $P_c$ , gained/lost during field-induced phase transition. Moreover, we demonstrate that under certain field-temperature conditions PMN-PT can retain its electrical field history and use it to kinetically accelerate its ferroelectric ordering. An explanation for the key difference between the phase transition dynamics in compositions near and far from the MPB is proposed and contextualized within prior publications.

## I. INTRODUCTION

PMN-PT is a condensed matter system that has multiple parameters affecting its macroscopic phase such as external electric fields, temperature, pressure, and the concentration of  $\text{PbTiO}_3$  [1–4]. Two phase diagrams can be constructed from these parameters: Temperature ( $T$ ) versus Concentration of  $\text{PbTiO}_3$  ( $x$ ) and Electric Field ( $E$ ) versus Temperature for a fixed concentration of  $x$  [5]. Fig. 1 shows an adapted  $T$ - $x$  phase diagram of PMN-PT which indicates the various types of induced ferroelectric states, distinguished by different crystalline lattice structures [6]. A region called the Morphotropic Phase Boundary (MPB) delineates different ferroelectric states by their crystallographic structure [6]. In Fig. 1, this is represented by Phase II. Prior literature has established that different ferroelectric modes in this region not only compete but also coexist in this region [7]. Thus, a PMN-PT crystal with a concentration  $x$  near the MPB is an excellent system to study the effects on macroscopic properties due to the competition and coexistence of multiple types of long-range ferroelectric order.

Yet, this is not the only length scale at which polar order exists within PMN-PT. PMN-PT is an engineered material where a regular relaxor,  $\text{Pb}(\text{Mg}_{1/3}\text{Nb}_{2/3})\text{O}_3$ , is doped with a concentration,  $x$ , of a regular ferroelectric,  $\text{PbTiO}_3$ . Although there is no single universally accepted definition of a relaxor, a typical relaxor exhibits three key properties. First, its dielectric response is diffuse, rounded, and dispersive in nature [9]. Second, there is no macroscopic change in its crystallographic structure when the system gains relaxor properties [9]. Third, the dielectric susceptibility does not follow the Curie-Weiss Law relation,  $\chi = \frac{C}{T-T_c}$ , as standard ferroelectrics do [9]. These properties can be explained by the formation

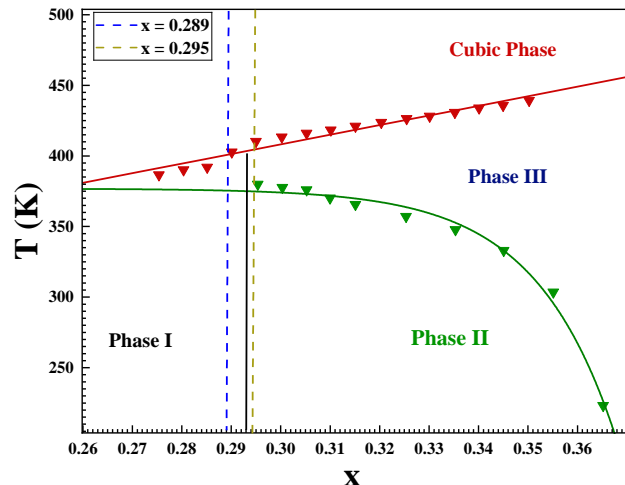


FIG. 1: An empirical concentration-temperature phase diagram for PMN-PT adopted from [8]. Phase II represents the Morphotropic Phase Boundary for PMN-PT. Phase I typically represents the Pseudocubic/Rhombohedral ferroelectric state, while Phase III typically represents the Tetragonal ferroelectric state. On the phase diagram, the colored dashed lines represent the concentration of each sample that was studied.

of local polar short-range order, known as Polar Nanoregions (PNRs), attributed to the off-center displacement of atoms within the unit cell [10]. These local, short-range polar structures lead to glassy behavior, where they are frozen in place below a freezing-temperature (derived from Vogel-Fulcher relations),  $T_f$  [11, 12].

The nature of field-induced ferroelectric phase transitions in relaxor ferroelectrics can be altered by varying parameters of the experimental protocols used to generate the phase transition. For example, in compositions of PMN-PT far from the MPB ( $x \sim 0.12$ ), as the cooling rate is reduced, the temperature where field-cooled ferroelectricity is reached increases [13], as shown

\* kolla@illinois.edu

in Fig. 3 (a). The electrical field history is another key factor that significantly affects features of field-induced phase transitions in relaxor ferroelectrics. In compositions near the MPB of  $\text{PbZn}_{1/3}\text{Nb}_{2/3}\text{O}_3\text{-PbTiO}_3$  (PZN-PT), it was shown that a prior field-cooled phase transition could be remembered in a subsequent zero-field cooling phase transition [14–16]. Similar memory effects were observed in other relaxor-ferroelectrics including  $\text{Sr}_{0.61}\text{Ba}_{0.39}\text{Nb}_2\text{O}_6$  doped with cerium (SBN-Cerium) [17]. Further neutron diffuse scattering measurements on PZN-PT revealed that under application of a moderately strong electrical field, short-range polar structures coexisted with macroscopic ferroelectric domains [18].

Though studied in other relaxor-ferroelectric systems, the field-induced ferroelectric phase transition dynamics in compositions of PMN-PT near its MPB is not well understood. To the extent of the authors' knowledge, there is currently an insufficient amount of literature that seeks to determine if the kinetics and dynamics of such phase transitions significantly differ in compositions of PMN-PT near and far from its MPB. In this paper, we will show that the behavior exhibited by field-induced ferroelectric phase transitions in compositions of PMN-PT near the MPB differ notably from the behavior exhibited in compositions of PMN-PT far from the MPB. Our principal results are three-fold. First, our results demonstrate that the electrical-field, temperature history dependence for PMN-PT compositions near and far from the MPB fundamentally differ. Second, our results suggest that the phase-transition dynamics exhibit kinetic dampening when aged in certain temperature regions, translating to notably delayed field-induced ferroelectric phase transitions. Third, our results show that this dampening behavior can be “overridden” under repetitive electrical field-temperature cycling. Additionally, we find an exotic “memory” effect, where PMN-PT compositions near the MPB can undergo ferroelectric phase transitions without requiring a concurrent application of an electrical field. This is only occurs when a certain electrical field-temperature induced history was induced on the composition.

## II. SAMPLE PREPARATION AND EXPERIMENTAL METHODOLOGY

In our experiments, we used two samples, with [111] orientations, where  $x = 0.289, 0.295$ . They are labeled by their respective. Each sample was grown by MSE Supplies using the Bridgman technique (akin to the sample used in [13]). Each PMN-PT sample was configured as a capacitor. A 100 nm Ag thick film was layered on top of 10 nm of Cr, prepared through in vacuum thin-film deposition to act as electrode plates deposited on top of PMN-PT samples. The electrode areas were approximately  $6.0 \text{ mm}^2$ , and thickness of the samples were approximately 0.5 mm. The sample-based capacitor system was mounted onto a measurement probe in a sealed cryo-

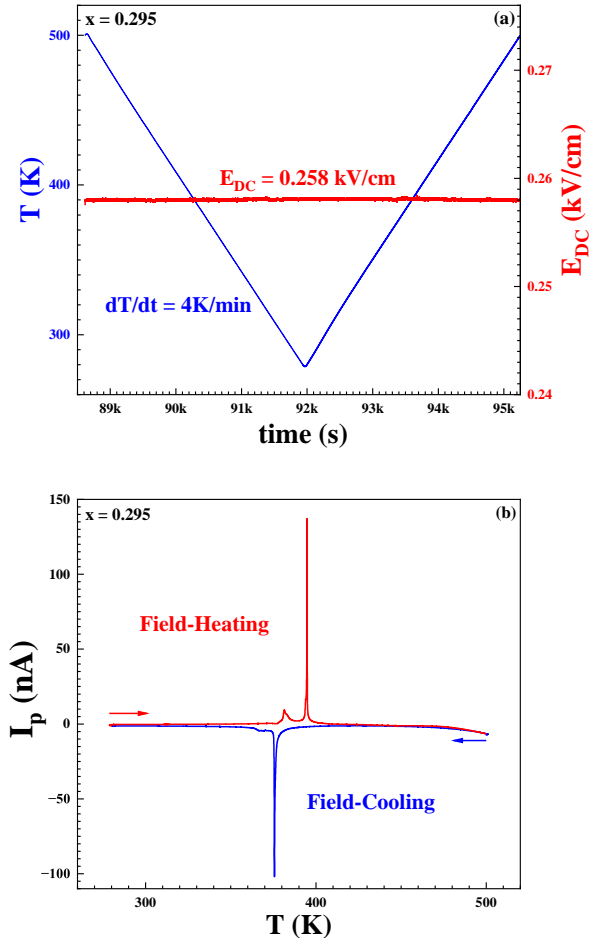


FIG. 2: (a) FC-FH Regime Protocol; (b) Polarization current responses during FC and FH.

stat chamber. AC and DC electrical fields were applied to the sample. The AC current response was measured by SR830 lock-in amplifier, which provided information on the dielectric susceptibility. The DC component of the current was measured by a digital voltmeter. The variation of the polarization was calculated by integrating the polarization current.

To determine the concentration of each sample, we cooled the samples at a fixed rate ( $\frac{dT}{dt} = 4 \text{ K/min}$ ) from  $T = 500 \text{ K}$  in the paraelectric region to  $T \leq 300 \text{ K}$  under concurrent application of a low strength AC electrical field ( $E_{AC} = 0.002 \text{ kV/cm}$ ). No DC electrical field bias was applied to the sample during the experiment. The real, linear dielectric susceptibility was measured during the entirety of the experiment, allowing us to plot it as a function of the sample temperature. After obtaining the temperature of peak dielectric susceptibility,  $T_{max}$ , we used an empirical formula provided in [8] for  $x < 0.5$ :

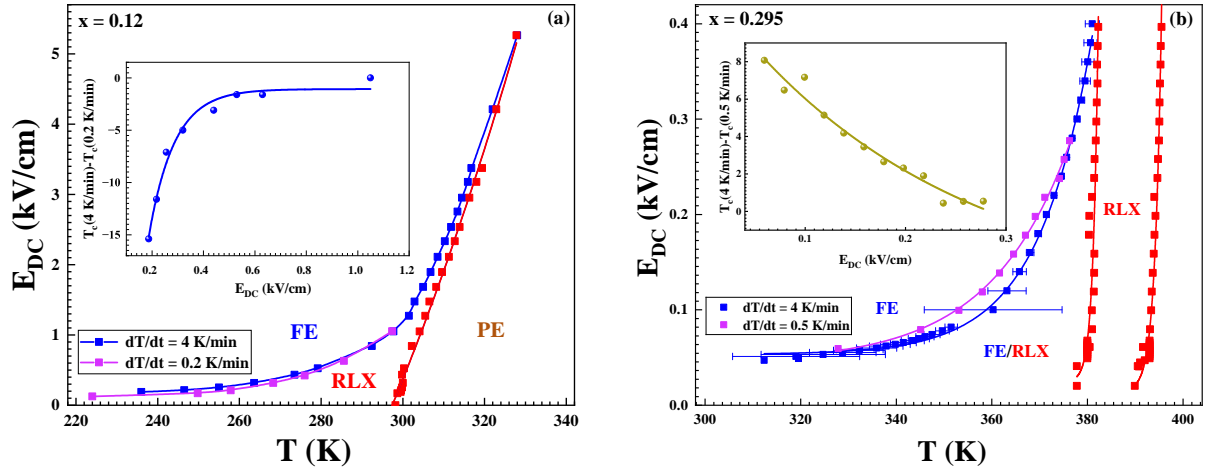


FIG. 3: Empirical field-induced temperature-electrical field phase diagrams are shown for (a) PMN-PT composition with  $x \sim 0.12$  (adopted from [13]) and (b) for PMN-PT composition with  $x \sim 0.295$ . Two cooling lines are plotted for two different cooling rates: 4 K/min and 0.5 K/min. The difference between these cooling lines is plotted as a function of DC electrical field strength in the insets.

$$x = \frac{T_{max} - 236}{528} \quad (1)$$

From this, we found the approximate concentrations of the samples we studied in this report. The concentrations of the samples are also marked on Fig. 1.

### III. RESULTS

#### A. Field-Cooling Regime

The field cooling (FC) and field heating (FH) regime is defined by the application of a DC field at high temperature and ramping the temperature down and up with the same value of the DC field. Above a certain threshold DC electrical field, PMN-PT will undergo a field-induced ferroelectric phase transition. The transition temperature was established by the polarization/depolarization current peaks. Our experimental investigations study how  $T_c$  changes due to different applied temperature-field histories in the FC-FH regime.

Fig. 2 (a) shows a typical FC experimental protocol. The polarization current spikes associated with a macroscopic field-induced ferroelectric phase transition in the Field-Cooling and Heating regime are provided in Fig. 2 (b). A singular polarization current spike is observed when the PMN-PT composition undergoes a transition from the relaxor to the ferroelectric phase. During the melting of the polarization, two polarization current spikes are observed, where one has a notably smaller amplitude but covers a broader temperature range. Through this experiment, the threshold electric-field  $E_{th}$  (mini-

mum electrical field require to observe ferroelectric transition) was determined. Next, this experiment was repeated at different strengths from 0 to 0.4 kV/cm. In addition, it was performed for two different cooling rates  $\frac{dT}{dt} = 0.5$  and 4 K/min. From the results of this experiment, an electrical field-temperature (T-E) phase diagram was constructed for each sample similar to Fig. 3 (a).

Fig. 3 compares the  $E$ - $T$  phase diagrams for the field-induced phases in the  $x = 0.295$  composition studied in this report to the  $x = 0.12$  composition studied in [13]. For the sample with  $x = 0.295$ , we observed two steps of melting of the ordered phase. In Fig. 3 (b), the cooling line for  $dT/dt = 0.5$  K/min is behind the cooling line for  $dT/dt = 4$  K/min in the  $x = 0.295$  sample. This is opposite of the behavior seen in the low-concentration sample  $x = 0.12$ , where the empirical cooling line for  $dT/dt = 0.2$  K/min is ahead of the  $dT/dt = 4$  K/min cooling line. The inset graphs of Fig. 3 also further quantify the behavior of the differences between the transition temperatures between the different cooling rates. This difference is eliminated as the strength of the electrical field is increased, asymptotically reaching zero.

These results primarily indicate that field-induced phase-transition dynamics in PMN-PT are strongly dependent on electrical field and temperature (field-temperature) history. There is a physical difference between cooling at different rates—it is how long the sample spends in a non-ferroelectric state. Given that the endpoint temperatures were fixed in our protocols, a sample that is cooled at  $dT/dt = 4$  K/min spends less time in a non-ferroelectric state compared to sample that is cooled at  $dT/dt = 0.5$  K/min. Hence, our results imply that more time-spent in a non-ferroelectric state can notably

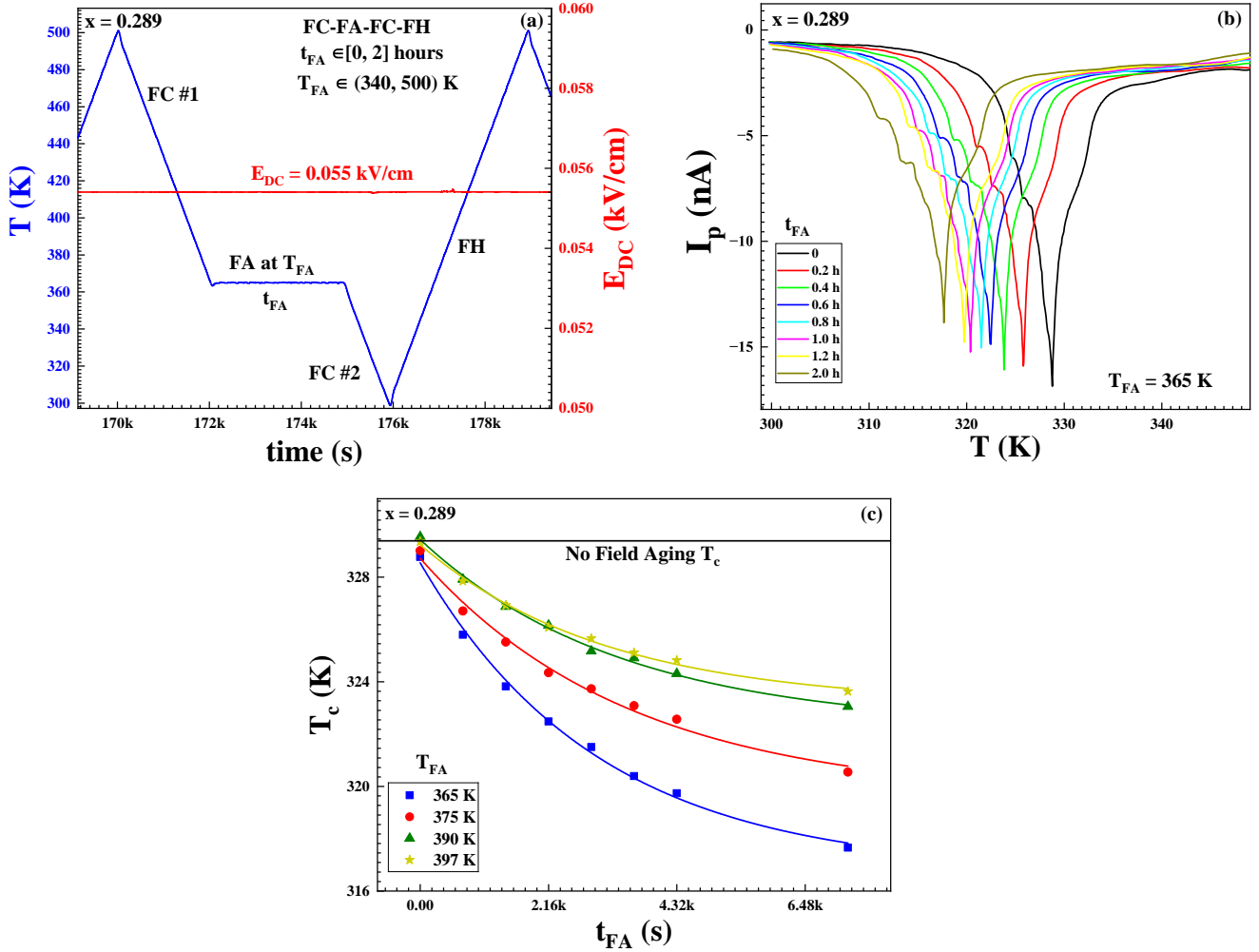


FIG. 4: (a) Intermediate Field-Aging step protocol is shown as temperature and external electrical field strength as functions of time. (b) The field-induced polarization current in FC#2 is plotted against the continuous measurement of temperature for different aging times ranging from 0 to 2 hours. (c) Characteristic curves of field-induced phase transition temperatures are plotted as a function of the aging time for four different aging temperatures.

change induced ferroelectric phase transition dynamics.

The next experiments critically examine the nature of the complex electrical field-temperature history dependence of phase transitions in this system. First, an additional intermediate isothermal aging step was added to the temperature cycle. The temperature of this field-aging step ( $T_{FA}$ ) and the time spent in the isothermal field-aging step ( $t_{FA}$ ) were varied in this experiment. Our goal was to understand spending more time in which temperature region was responsible for the observed significant temperature lag between fast and slow cooling rates in the  $E$ - $T$  phase diagram.

In Fig. 4, the protocol of the experiment (a), examples of raw data (b), and the results of significant reduction of the transition temperature  $T_c$  (c) are shown. It is also shown that as the aging temperature is decreased to near the no-aging transition temperature, the rate at which  $T_c$  decreases notably increases. This result implies that ag-

ing in a temperature region below the two melting lines in the phase diagrams (see Fig. 3) significantly dampens the kinetics in field-cooled phase transitions. In addition, the observed temperature lag gets larger as  $t_{FA}$  increases. It is probable that formation of glassy order in the field-aging step is responsible for this phenomena. Spending  $t_{FA}$  in the aging step likely determines the rigidity of glassy order formed, while performing the aging at  $T_{FA}$  could determine how quickly the glassy order is formed in the aging step.

Our second investigation determined if cooling from different temperatures on the phase diagram significantly impacted  $T_c$ . The FC-FH cycles were performed with step-by-step reduction of the maximum annealing temperature as shown in Fig. 5 (a)—denoted by  $T_{ret.}$ . Another interesting point is that the ratio of time spent in the ferroelectric state to the time spent in non-ferroelectric states increases as  $T_{ret.}$  is reduced.

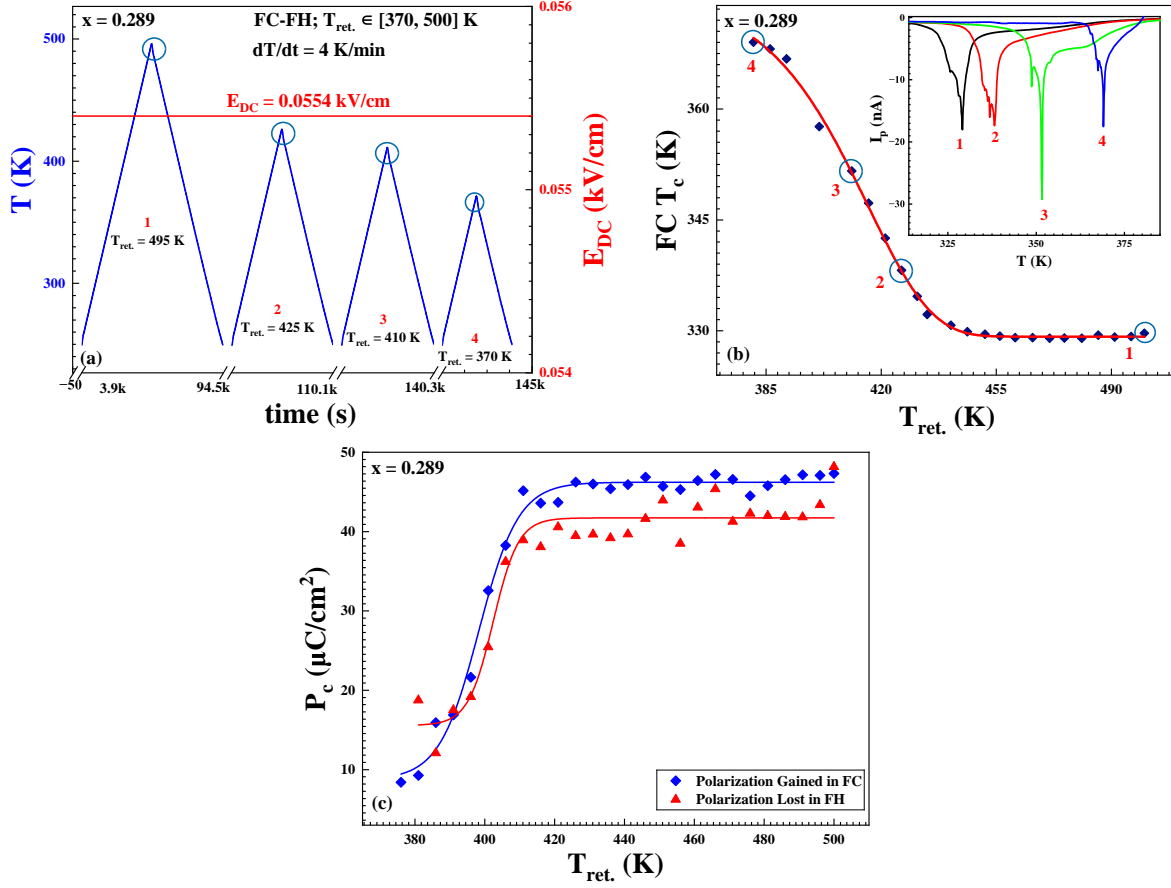


FIG. 5: (a) Certain time slices of the different return point experimental protocol are shown. (b) The empirical field-induced ferroelectric phase transition temperature is plotted against the return point temperatures. Four return point temperatures are circled in both (a) and (b). The inset graph plots the induced polarization current for the four circled points against temperature. (c) The polarization gained (marked in blue) and lost (marked in red) in field-induced phase transitions is graphed as a function of return point temperature.

Hence, this experiment investigated how the polarization lost/gained in the heating/cooling step varied across different temperature regions.

From Fig. 5 (b), it is clear that the FC transition temperature rapidly increases with decreasing of annealing temperature  $T_{ret.}$  from 440 K and remains almost constant when  $T_{ret.}$  is higher than 440 K. The range of the temperature shift in  $T_c$  is approximately  $\Delta T \sim 40$  K, demonstrating a significant difference between field-induced phase transitions with different starting high-point temperatures. As seen in Fig. 5 (c), the polarization gained and lost,  $P_c$ , remains relatively constant in  $T_{ret.}$  from 420 to 500 K. Below  $T \leq 420$  K,  $P_c$  drastically drops, following a similar logistic trend evident in Fig. 5 (b). This indicates that not all the polarization is melted when field-heating to a temperature near the melting lines—the sample has retained a fraction of the saturated polarization. As indicated by the shift in  $T_c$ , it is likely that retained polarization can kinetically accelerate the induced phase transition. In addition, a

temperature lag between where the sharp decrease in  $P_c$  and increase  $T_c$  happen is observed. This suggests that the retention of polar order may occur at the microscopic scale, potentially acting as a trigger for this phenomena.

## B. Zero Field-Cooling Regime

The zero-field cooling (ZFC) regime is specified by cooling a sample in zero field to the temperature below the freezing line in Fig. 3 and applying the DC electrical field at that fixed temperature. The transition to the long-range induced ferroelectric state appears not instantly but after some delay time,  $\tau_{ZFC}$  which depends on the temperature and value of the DC field [19]. A set of ZFC experiments (analogous to the FC regime) was performed to study how  $\tau_{ZFC}$  depends on the field-temperature history of the system.

Our experiment focused on investigating  $\tau_{ZFC}$  as a function of isothermal relaxation temperature ( $T_{ZFC}$ ) for

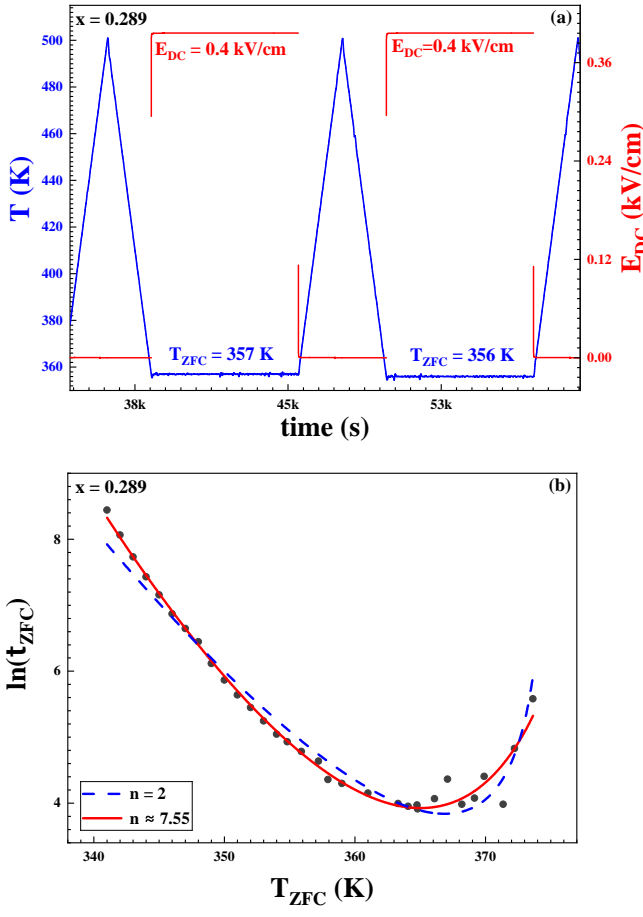


FIG. 6: (a) The temperature-field protocol for the regular zero-field cooling/heating regime is shown as electrical field and temperature plotted as functions of time.  $T_{ZFC}$  was varied between 340 and 375K. (b) The natural logarithm of  $\tau_{ZFC}$  is plotted as a function of  $T_{ZFC}$ . Two fits are plotted according for different exponent  $n$  in Equation 2.

a fixed value of applied  $E_{DC}$  (see Fig. 6 (a)). On Fig. 6 (b),  $\tau_{ZFC}$ , shows a dramatic increase in  $\tau_{ZFC}$  for low temperature  $T_{FA}$ . In this experimental protocol,  $\tau_{ZFC}$  can also be postulated as a nucleation lag time as presented in [20]. In this context, the observed time-dependence indicates a deviation from the typical Arrhenius-like behavior similar to the trend observed in compositions of PMN-PT at  $x = 0.20$  [20]. The data was fit to the following equation:

$$\ln\left(\frac{\tau}{\tau_0}\right) = \frac{T_1}{T} - n \ln\left(1 - \frac{T}{T_C}\right) \quad (2)$$

In this equation,  $\tau_0$  and  $T_1$  are fit parameters, while  $n$  represents the rate of divergence of the nucleation lag time. This choice of this fit stems from the leading order

approximation ( $\Delta G(T) \sim [T - T_C]$ ) of the classical Arrhenius homogeneous nucleation theory prediction [21]:

$$\tau \propto \frac{\exp \frac{B}{kT}}{\Delta G(T)^2} \quad (3)$$

In Equation 3,  $B$  represents the Arrhenius Barrier height,  $k$  is the Boltzmann constant, and  $\Delta G(T)$  is the bulk free-energy difference between the ordered and disordered phases [20]. If the nucleation process is described by Equation 3, then  $n$  should be equal to 2 in Equation 2.

Our result indicates that the nucleation lag time only qualitatively follows the temperature of Equation 3. This

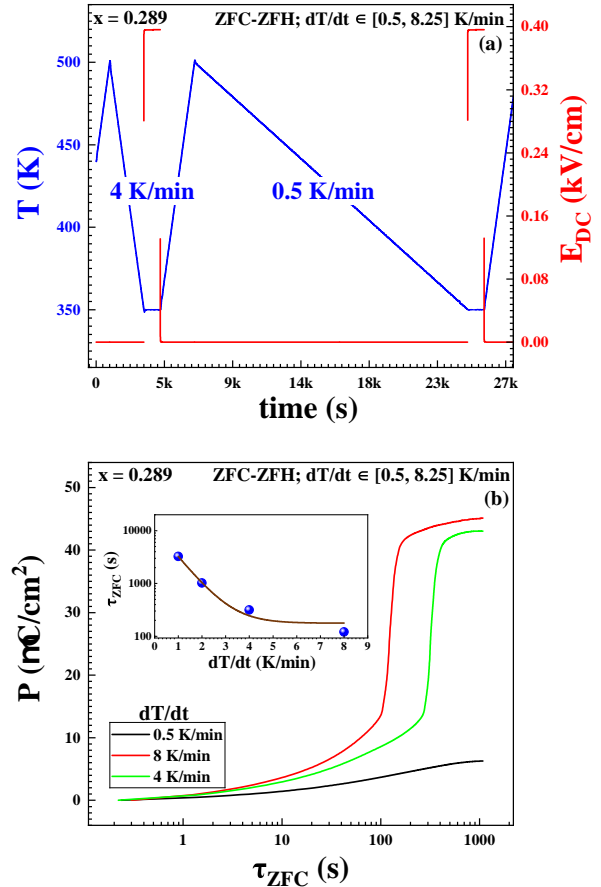


FIG. 7: (a) The empirical protocol for performing zero-field cooling/heating is shown for two cooling rates:  $dT/dt = 4$  K/min and 0.5 K/min. (b) The polarization is plotted as a continuous function of time on a log base-10 scale during the ZFC-relaxation step for three cooling rates:  $dT/dt = 0.5, 4$ , and 8 K/min. The inset shows the dependence of  $\tau_{ZFC}$  for all experimentally tested cooling rates.

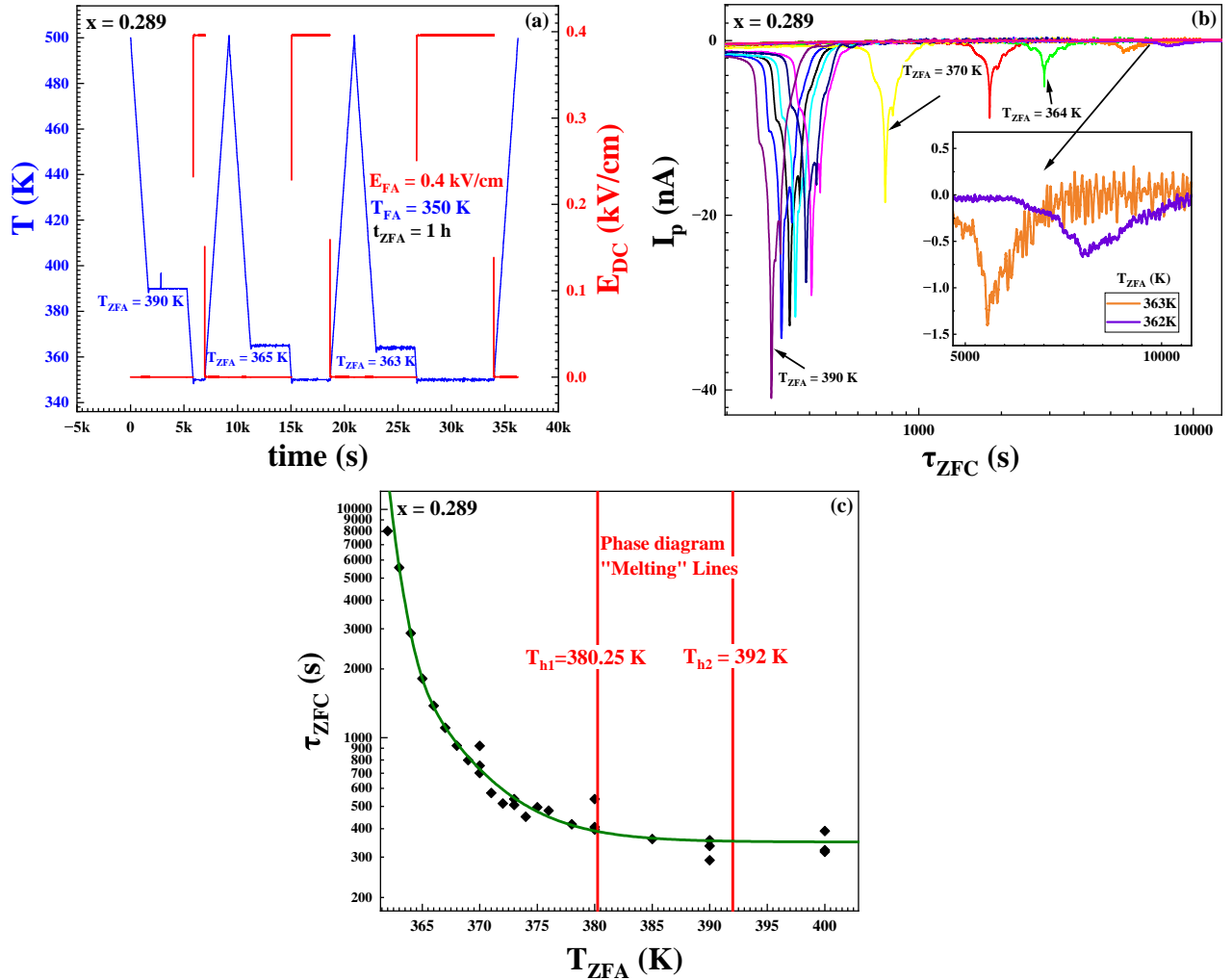


FIG. 8: (a) The intermediate zero-field aging step experimental protocol is plotted as temperature and DC electrical field strength as functions of time. The zero-field aging duration,  $t_{ZFA}$ , was fixed at an hour and the field aging temperature,  $T_{FA} = 350$  K, was fixed for all experiments. (b) The polarization current is plotted against the time delay until ferroelectricity,  $\tau_{ZFC}$  for varying  $T_{ZFA}$ . A zoomed-in inset plot is provided for polarization currents with  $T_{ZFA} = 362$  and  $363$  K . (c)  $\tau_{ZFC}$  is graphed against  $T_{ZFA}$ .

is in accordance with prior work on PMN-PT compositions with  $x = 0.20$  [20]. The  $n = 2$  fit fails to capture to low-temperature data as the rate of divergence in  $\tau_{ZFC}$  is much steeper than expected. When  $n$  was made an adjustable fitting parameter, the best fit found was for  $n \sim 7.5$ . This exponent is larger than any best-fit exponent found in PMN-PT compositions  $x = 0.12$  and  $x = 0.2$  [20]. This is preliminary evidence of enhanced slowing of induced phase-transition dynamics in compositions of PMN-PT near the MPB. The system exhibits also rapid  $\tau_{ZFC}$  divergence for  $T_{ZFC} > 365$  K. This is within expectations as a non-ferroelectric state can provide an increase in entropy that outweighs the energetically-favorable ferroelectric state.

Next, the ZFC experiment was repeated with vary-

ing cooling rates while approaching the ZFC temperature. Fig.7 (b) shows the dependence of polarization of the sample on ZFC cooling rate. The polarization was calculated as a function of time from the start of the field-aging step to every data-acquired point in time. The delay time,  $\tau_{ZFC}$ , significantly increased as the cooling rate decreased. In all ZFC experiments, we observe a polarization creep to a critical polarization (typically 1/3 of the saturated polarization), which is followed by an avalanche-like phase transition into the ferroelectric state. As seen in the inset of Fig.7 (b), this polarization creep rate is strongly dependent on the cooling rate. Approaching  $T_{ZFC}$  at a slower cooling rate also slowed the polarization creep to the critical polarization. The natural tendency to form short-range glassy frozen order

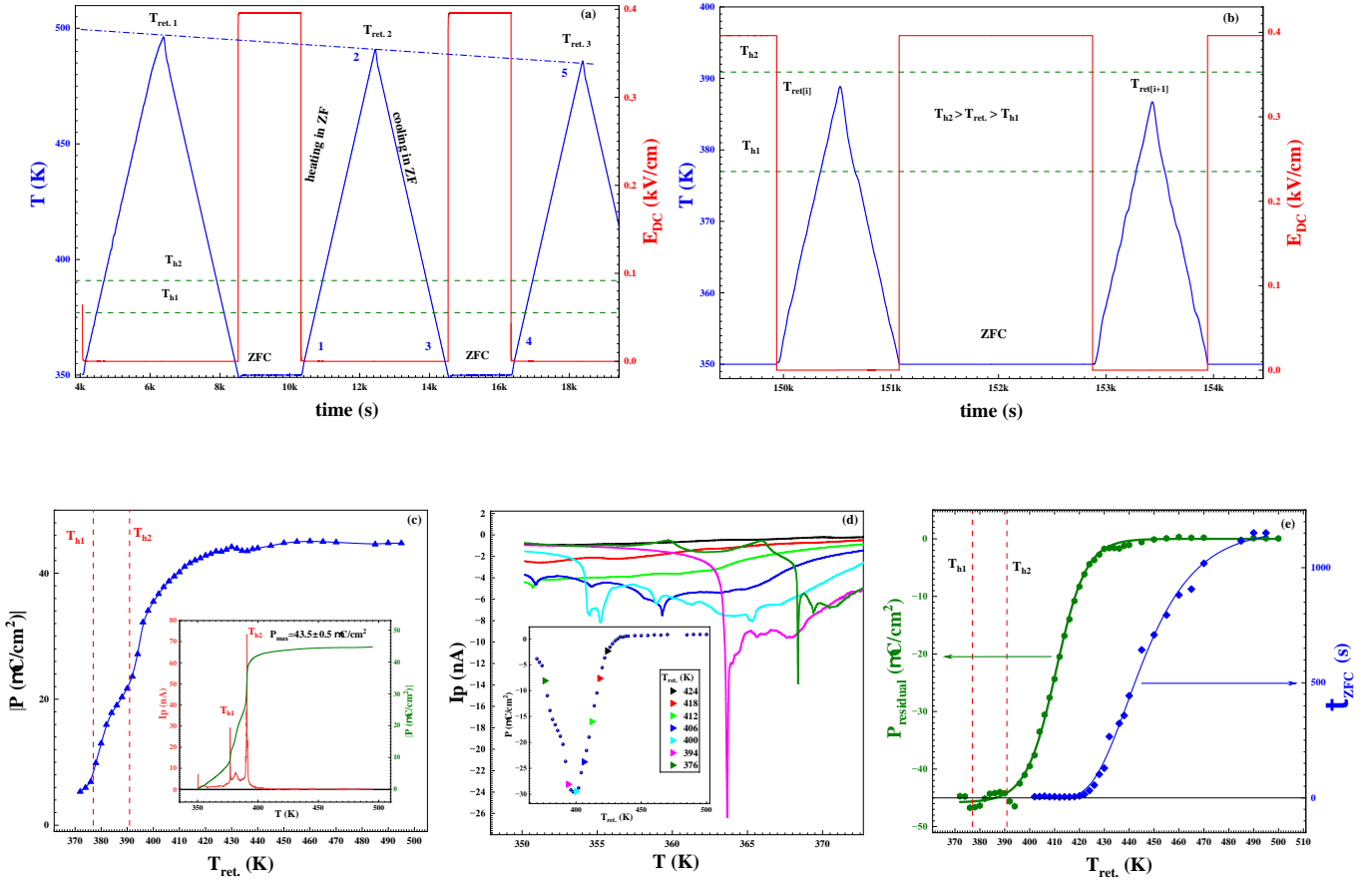


FIG. 9: ZFC Different Return Point Temperature experimental protocol is shown for  $T_{ret.} \gg T_{h1} \& T_{h2}$  (a) and  $T_{h1} < T_{ret.} < T_{h2}$  (b). (c) Melted Polarization in heating step is plotted as a function of the return temperature. (d) Polarization Currents in the no-field cooling step are plotted for different return point temperatures. In the inset graph, the polarization gained in this step is plotted for all return point temperatures. (e) The residual polarization after every ZFC cycle and ZFC relaxation time  $\tau_{ZFC}$  are displayed for all return point temperatures.

has been previously argued in low-concentration compositions of PMN-PT [13, 22]. Hence, it is likely the system experiences an enhanced competition between the formation of glassy and ferroelectric order in slower-cooling rate experiments, where more time is spent in a non-ferroelectric state.

A Zero-Field Intermediary Aging Step experiment was performed to study this possibility, testing if aging in a particular region of the FC-FH phase diagram significantly impacted  $\tau_{ZFC}$ . The protocol of this experiment is shown in Fig. 8 (a). There are two isothermal aging steps. The first aging step was done with no external electrical field applied. The second aging step is the transition inducing step—similar to the standard ZFC experiment described above. The variable parameter in this experiment was the temperature of first zero field aging,  $T_{ZFA}$  (refer to Fig. 8 (a)).

The result of this experiment clearly show significant increasing of the delay time,  $\tau_{ZFC}$ , starting below the temperatures of the two melting lines. Raw data of the polarization current spikes observed in the ZFC relaxation—after additional step of aging at different  $T_{ZFA}$  temperatures—is shown in Fig. 8 (b), and final results of this experiments are presented in Fig. 8 (c). This result is coherent with the different cooling rate experiment and shows that spending more time in temperatures below the melting temperatures fundamentally impacts the transition to the long-range ordered phase in the ZFC regime. In the region below the melting lines—representative of the relaxor state—aging significantly quenched the phase transition dynamics. This narrows the temperature location to the relaxor state where slowed induce-phase transition dynamics arise from.

Finally, a ZFC different return point temperature experiment was performed to determine the cooling/heating behavior from different temperatures of ZFC phase transitions. Fig. 9 (a) and (b) shows the experimental protocols for two temperature regions: above and between the melting lines. Starting at point 1 on Fig. 9 (a), the sample is fully polarized from the previous ZFC relaxation step. From the observed depolarization current, the polarization lost in each heating step can be approximated. It is important to note that the maximum obtainable polarization can be estimated when the sample is heated up to  $T_{ret.} = 500$  K. Fig. 9 (c) shows the amount of polarization lost after heating the sample to  $T_{ret.}$ , with the inset focusing on the depolarization record for  $T_{ret.} = 500$  K. It is clear that the sample does not lose all polarization even when it is heated over both melting temperatures ( $T_{h1}$  and  $T_{h2}$  on the figure). After heating to  $T_{ret.}$  at point 2, the next step is to cool back to the ZFC relaxation temperature  $T_{ZFC} = 350$  K (point 3). Fig. 9 (d) shows the polarization currents obtained in the no-field cooling steps. It is evident that ferroelectric self-ordering is occurring without the application of an external electrical field. This ferroelectric ordering may be coerced due to the unmelted polarization. The inset graph shows the polarization gained during the cooling steps from different  $T_{ret.}$ . The polarization gained in the step depends on  $T_{ret.}$ , where a maximum polarization gained in this step is located at  $T_{ret.} = 400$  K.

The last step of the cycle is performing the ZFC-relaxation step (from point 3 to point 4). Given the not all polarization is melted away in the heating step and some polarization is gained in the cooling step, the ZFC-relaxation step starts with non-zero polarization. Hence, Fig. 9 (e) shows the residual polarization of the sample prior to performing the ZFC-relaxation step (green line). The residual polarization was calculated by subtracting the polarization lost in the heating step from the maximum system polarization and then adding this quantity to the polarization gained in the cooling step. Fig. 9 (e) also shows the ZFC delay time as a function  $T_{ret.}$  (blue line). This data could only be obtained up to  $T_{ret.} = 400$  K due to our limited second time-resolution. Given that  $\tau_{ZFC}$  decreases rapidly at much higher  $T_{ret.}$ , it is clear that even a small amount of residual polarization can significantly accelerate the transition to the ferroelectric ordered phase during the ZFC step. Specifically, the system does not require a macroscopic polarization to generate this kinetic acceleration, hinting that this phenomena origins lie within the short-range polar order.

#### IV. DISCUSSION

The key interpretation of our experiments is that the dynamics of induced ferroelectric transition in compositions of PMN-PT near its morphotropic phase boundary (MPB) exhibit a field-temperature history dependence that significantly differs to the history dependence ex-

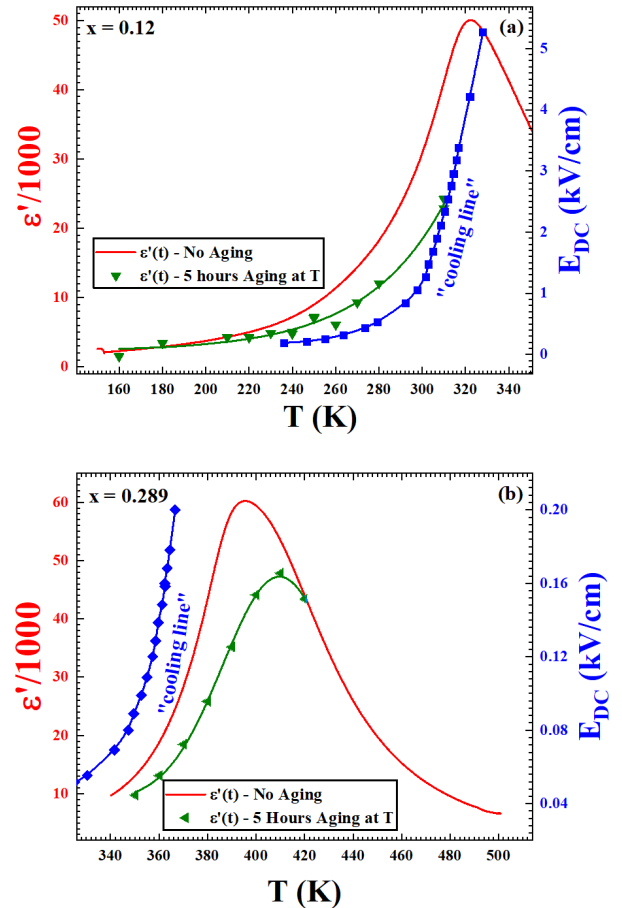


FIG. 10: Real component of the scaled dielectric susceptibility,  $\epsilon'(T)$  is plotted for (a) no-aging continuous measurement and (b) after 5 hours of aging at fixed  $T$ . “Cooling Line” refers to the field-induced ferroelectric transition temperatures on Fig. 3. The  $x = 0.12$  data was adopted from [13] and [23].

hibited in compositions far below the MPB. In our experiments, we controlled the history-profile of these compositions in two different regimes: The time spent in non-ferroelectric and ferroelectric states. Hence, we split this discussion into these two regimes and describe potential mechanisms responsible for the observed impacts on field-induced ferroelectric phase transitions.

##### A. Formation of Glassy Order in Non-Ferroelectric State

The FC-FH phase diagrams indicate that as compositions of PMN-PT near the MPB spend more time in a non-ferroelectric state, the field induced transition temperature decreases (see Fig. 3 (b)). This ob-

servation was further refined by the aging experiments where it was found that aging at a temperature below the melting-temperatures also significantly decreased the field-induced transition temperature (see Fig. 4 (c)).

These observations are counterintuitive and prompt the following question: Specifically, why does the ferroelectric transition temperature increase for slower cooling rates for compositions with  $x = 0.12$  but decrease for compositions with  $x \sim 0.30$  (refer to Fig. 3)—where there is more ferroelectric dopant to guide the system to a ferroelectric state? Fig. 10 hints at the explanation difference between low and high concentration induced transition dynamics. It shows the dielectric susceptibility as a function of temperature,  $\epsilon'(T)$  temperature in two different regimes (1) no-aging, continuous and (2) after 5 hours of aging at fixed temperature,  $T$ . Comparing Fig. 10 (a) and (b), it is clear that the dielectric aging predominantly occurs in different temperature intervals for different concentrations: For the composition  $x = 0.12$ , the aging occurred below the field-induced ferroelectric transition line, whereas for  $x = 0.289$ , aging occurred well above it. Aging of the dielectric susceptibility response can represent the formation of glassy-order in the composition, which is typically indicated by an inverse-power law of the dielectric loss response during the aging step [23]. Preliminary analysis indicates that the dielectric loss response in  $x = 0.289$  (not presented here) does indeed follow the “spin-glass like” aging response found in low-concentrations of PMN-PT [23]. However, special in-situ barkhausen noise and aging experiments are required to verify this.

This allows us to offer an appealing interpretation that potentially resolves this inconsistency. At low-concentration  $x = 0.12$ , the induced phase transition will remain unimpeded even in slow-cooling as minimal glassy order is formed above  $T_c$ . As described in [13], once the initial symmetry has been broken, the system will experience gradual polarization creep to the ferroelectric state. This increases  $T_c$  when the cooling rate is decreased.

However, for  $x = 0.289$ , the induced phase transition will be inhibited by the formation of glassy order in the non-ferroelectric state. To elucidate this point, we consider the system’s dynamics through the evolution of its free-energy. When the system’s temperature is varied slowly or completely fixed for a certain duration of time in a non-ferroelectric region, the free-energy landscape available to the system should evolve slowly as well. It has been previously argued that the presence of random, anisotropic quenching fields could be responsible for a relaxor state—a source to prevent the formation of long-range ferroelectric order [24], [25]. Similar to spin-glasses, the free-energy terrain could be rugged, including many metastable local free-energy minima valleys separated by large activation barriers [26, 27]. In nearly quasi-static cooling or isothermal aging in the non-ferroelectric state, it is likely that the system finds the formation of glassy-order as a local free-energy minima.

Trapped in this local well, a larger activation energy

would be required to undo the glassy-state and undergo a field-induced phase transition. This could act as the source of the observed lag, where the system has to be provided extra energy to freely evolve away from this local minima before it is able to undergo the phase-transition dynamics. Physically speaking, the external electrical field may need to first give small polar units (associated with the glassy-state) the mobility to reorient themselves and combine with existing long-range ferroelectric order. In rapid cooling, it is likely that minimal glassy-order is formed due to the rapid time evolution of the free-energy landscape, preventing the system from being trapped in any singular local free-energy minima. Hence, it does not undergo this extra melting step and no delay is observed.

While this interpretation neatly accounts for the results of the ZFC Aging Experiments (refer to Fig. 8 (c)), it still remains questionable whether a glassy-state can be formed even when an external electrical field is applied to the system. Fig. 4 (c) seems to suggest that it is possible for some formation of glassy order in isothermal field-aging. Yet, the formation of a glassy-state may be strongly dependent on the temperature and strength of the external electrical field. A stronger competition between the formation of glassy and ferroelectric state is likely to occur. As the applied electrical field strength is increased, the coupling of local polar order to the external field should exceed the coupling to the quenching field, preventing the formation of any glassy order in the system. This could explain why the temperature lag between the slow and fast cooling line on Fig. 3 eventually vanishes.

While the effects due to the formation of a glassy state have been addressed, it remains unclear why it is preferred at higher temperatures in PMN-PT compositions near the MPB. However, we offer a rudimentary conjecture based on the volatile nature of the MPB. At a fundamental level, PMN-PT has two competing polarized lattice structures: PT naturally prefers a Tetragonal structure, while PMN prefers an induced Rhombohedral structure. Hence, it is possible that the systems near the MPB experience a lattice-based structural frustration due to the competition between the two polar structures. There is precedence for this concept as the  $T$ - $x$  phase diagram near the MPB is not well-defined, with different publications finding different ferroelectric modes [4, 6]. This unresolved phase-diagram mystery has been attributed due to the competition of the tetragonal and rhombohedral lattice structure. Given that the source of anisotropic quenching fields is compositional in nature [25, 28, 29], it is reasonable to conjecture that this lattice-based structural frustration can lead to enhanced anisotropic quenching in the non-ferroelectric state for compositions of PMN-PT near the MPB. Fig. 10 implies the formation of glassy-state at much higher temperatures for  $x \sim 0.30$ , which could be an effect of enhanced anisotropic quenching near the MPB.

Finally, a second inconsistency is that the natural ten-

dency to form a glassy-ordered state should no longer hold true as  $x$  approaches 0.4, where the system acts like a true ferroelectric. It is unclear at which concentration will this phenomena no longer be observed, signaling the shift from relaxor-ferroelectric to standard ferroelectric behavior. Further investigations into samples  $0.3 < x < 0.4$ —using a similar set of experimental protocols—are currently being performed to study this point in greater depth.

## B. Kinetic Acceleration of Ferroelectric Ordering

In addition to revealing the field-temperature history dependence in the non-ferroelectric state, our results also unveiled an interesting phenomenon for the induced phase-transition dependence on field-temperature history in the ferroelectric state. Specifically, the FC different return point temperature experiment revealed that for annealing temperatures near the empirical cooling line, the system underwent induced phase transitions at higher temperatures. In the ZFC regime, the system underwent phase transitions quicker in the ZFC-relaxation step. Additionally, the system exhibited a memory effect, where it retained some polarization information regarding about prior ferroelectric domains. In the ZFC regime, we see an additional effect where the system can use this retained polarization to self-organize ferroelectric order in zero external electrical field.

These results could be explained by a mechanism similar to the repoling process found in the relaxor-ferroelectric SBN-Cerium [17] and PZN-PT (also near its MPB) [14], [18]. In the FC regime, it is likely that the system may not be able to retain prior polarization information beyond certain return point temperature. On Fig. 5 (b), this certain return point temperature is  $T_{ret.} \sim 440$ K. However, below this return point temperature, it is possible that short-range polar order start to retain polar orientations from prior ferroelectric domains. Fig. 9 (e) supports this idea as even though the residual polarization is nearly 0 from 430 to 500 K,  $\tau_{ZFC}$  has dropped nearly two orders of magnitude. As  $T_{ret.}$  is subsequently reduced, more short-range polar order may retain their “unmelted” polar orientations. This retained short-range polar order may couple with depolarized neighbors, enabling a cooperative interaction to realign them to their prior polarization orientation. In the ZFC regime, this coupling to the melted order could also facilitate the self-organization into prior domain orientations, potentially explaining the zero-field polarization currents seen in Fig. 9 (d).

Eventually, the system will begin to retain macroscopic amounts of polarization in the form of unmelted polar

domains. Once macroscopic domains are not completely melted, the variational polarization gained and lost in different steps of the thermal cycle should decrease rapidly. There are three key results that support this claim. First, Fig. 5 shows that both polarization gained and lost substantially drops for  $T_{ret.} < 410$  K. Second, Fig. 9 (e) shows that there is substantial residual polarization prior to the ZFC-transition step, leading to a reduction in the possible polarization gained in the this step. Third, the inset plot Fig. 9 (d) shows that the polarization gained in the cooling step quickly approaches zero after reaching a maximum at  $T_{ret.} = 400$  K. Once  $T_{ret.} < T_{h1}$ , it is likely that there will be no noticeable variation of the polarization in the thermal cycle as the temperature variation does not exit the ferroelectric temperature region.

Yet, this proposed mechanism remains incomplete without answering the following question: What enables this retention process to begin in the non-ferroelectric state? First, it is likely that the external electrical field is responsible for the initial step, directly allowing it act as a source to repole short-range order. The non-ferroelectric state of PMN-PT is characterized by a complex entropic-energy competition, which is parameterized by the temperature and external electrical field. It is feasible that at some annealing temperature, the energy contribution from the external electrical field is strong enough to only embed previous polarization information into the short-range polar order after the ferroelectric order has been completely melted. From this perspective, these results can be interpreted as follows: until what temperature in the non-ferroelectric region, can an external electrical field help the system retain its polar order? Further diffuse neutron scattering measurements could be useful to confirm this explanation.

Finally, it is also important to characterize the stability of the ferroelectric order formed in the no-field cooling steps. This remains a focal point of our current investigations. Understanding the stability of the residual polarization above the melting temperatures is imperative to characterize the conditions under which ferroelectric phases are stable. This is linked to our investigations into PMN-PT compositions with  $x > 0.30$ , where the stability of the ferroelectric ordered phases remains unresolved.

## ACKNOWLEDGMENTS

We would like to thank students from the Fall 2025 semester of Physics 403: Modern Experimental Physics Laboratory course at the University of Illinois at Urbana-Champaign (UIUC), who worked on relevant data-collection of the final results. This work was sponsored by the Department of Physics at UIUC.

---

[1] H. Wu and R. Cohen, Electric-field-induced phase transition and electrocaloric effect in pmn-pt, Phys. Rev. B

96, 054116 (2017).

[2] B. Noheda, D. Cox, G. Shirane, J. Gao, and Z.-G. Ye, Phase diagram of the ferroelectric relaxor  $(1-x)\text{PbMg}_{1/3}\text{N}_{2/3}\text{O}_3-(x)\text{PbTiO}_3$ , *Phys. Rev. B* **66**, 054104 (2002).

[3] M. Ahart, S. Stanislav, O. Shebanova, D. Ikuta, Z.-G. Ye, H. Mao, R. Cohen, and R. J. Hemley, Pressure dependence of the monoclinic phase in  $(1-x)\text{PbMg}_{1/3}\text{N}_{2/3}\text{O}_3-(x)\text{PbTiO}_3$ , *Phys. Rev. B* **86**, 224111 (2012).

[4] I.-H. Kim, I.-H. Kim, S.-G. Im, and K.-O. Jang, A phenomenological study on temperature-concentration-electric field phase diagram of relaxor ferroelectrics pmn-pt single crystals, *Physica B Condens. Matter* **639**, 413961 (2022).

[5] M. Davis, D. Damjanovic, and N. Setter, Electric-field-, temperature-, and stress-induced phase transitions in relaxor ferroelectric single crystals, *Phys. Rev. B* **73**, 014115 (2006).

[6] Y. Guo, H. Luo, D. Ling, H. Xu, T. He, and Z. Ye, The phase transition sequence and the location of the morphotropic phase boundary region in  $(1-x)[\text{PbMg}_{1/3}\text{N}_{2/3}\text{O}_3]-(x)\text{PbTiO}_3$  single crystal, *J. Phys.: Condens. Matter* **15** (2003).

[7] H. Zhang, X. Lu, R. Wang, C. Wang, L. Zheng, Z. Liu, C. Yang, R. Zhang, B. Yang, and W. Cao, Phase coexistence and landau expansion parameters for a  $0.7\text{PbMg}_{1/3}\text{N}_{2/3}\text{O}_3-0.3\text{PbTiO}_3$ , *Phys. Rev. B* **96**, 054109 (2017).

[8] D. Zekria, V. A. Shuvava, and A. M. Glazer, Birefringence imaging measurements on the phase diagram of  $\text{PbMg}_{1/3}\text{N}_{2/3}\text{O}_3-\text{PbTiO}_3$ , *J. Phys.: Condens. Matter* **17**, 1593 (2005).

[9] E. L. Cross, Relaxor ferroelectrics: An overview, *Ferroelectrics* **151**, 305 (1993).

[10] B. Gerald and F. Dacol, Soft phonons in a ferroelectric polarization glass system, *Solid State Commun.* **58**, 567 (1986).

[11] A. Levstik, K. Zdravko, C. Filipič, and R. Pirc, Glassy freezing in relaxor ferroelectric lead magnesium niobate, *Phys. Rev. B* **57**, 1 (1998).

[12] M. Delgado, E. Colla, P. Griffin, M. Weissman, and D. Viehland, Field dependence of glassy freezing in a relaxor ferroelectric, *Phys. Rev. B* **79**, 140102(R) (2009).

[13] E. Colla, D. Vigil, J. Timmerwilke, M. Weissman, D. Viehland, and D. Brahim, Stability of glassy and ferroelectric states in the relaxors  $\text{PbMg}_{1/3}\text{Nb}_{2/3}\text{O}_3$  and  $\text{PbMg}_{1/3}\text{Nb}_{2/3}\text{O}_3-12\%\text{PbTiO}_3$ , *Phys. Rev. B* **75**, 214201 (2007).

[14] G. Xu, P. Gehring, and G. Shirane, Persistence and memory of polar nanoregions in a ferroelectric relaxor under an electric field, *Phys. Rev. B* **72**, 214106 (2005).

[15] S. Farnsworth, E. Kisi, and M. Carpenter, Elastic softening and polarization memory in pzn-pt relaxor ferroelectrics, *Phys. Rev. B* **84**, 174124 (2011).

[16] Y. Wang, D. Wang, G. Yuan, H. Ma, F. Xu, J. Li, D. Viehland, and P. Gehring, Fragile morphotropic phase boundary and phase stability in the near-surface region of the relaxor ferroelectric  $(1-x)\text{PbZn}_{1/3}\text{N}_{2/3}\text{O}_3-(x)\text{PbTiO}_3$ : [001] field-cooled phase diagrams, *Phys. Rev. B* **94**, 174103 (2016).

[17] T. Granzow, T. Woike, M. Wöhlecke, M. Imlau, and W. Kleemann, Polarization-based adjustable memory behavior in relaxor ferroelectrics, *Phys. Rev. Lett.* **89**, 1 (2002).

[18] G. Xu, P. Gehring, and G. Shirane, Coexistence and competition of local- and long-range polar orders in a ferroelectric relaxor, *Phys. Rev. B* **74**, 104110 (2006).

[19] E. Colla, E. Koroleva, N. Okuneva, and S. Vakrushev, Long-time relaxation of the dielectric response in lead magnoniobate, *Phys. Rev. Lett.* **74**, 1681 (1995).

[20] E. V. Colla, J. R. Jeliazkov, M. B. Weissman, D. D. Viehland, and Z.-G. Ye, Kinetics of nucleation of the ferroelectric transitions in  $\text{PbM}_{1/3}\text{Nb}_{2/3}\text{O}_3$  and  $\text{PbMg}_{1/3}\text{Nb}_{2/3}\text{O}_3-12\%\text{PbTiO}_3$ , *Phys. Rev. B* **90**, 024205 (2014).

[21] V. Fokin, E. Zanotto, N. Yuritsyn, and J. Schmelzer, Homogenous crystal nucleation in silicate glasses: A 40 years perspective, *J. Non-Crys. Solids* **352**, 2681 (2006).

[22] E. Colla, P. Griffin, M. Delgado, M. Weissman, X. Long, and Z.-G. Ye, Polarization-independent aging in the relaxor  $0.92\text{PbMg}_{1/3}\text{Nb}_{2/3}\text{O}_3 - 0.08\text{PbTiO}_3$ , *Phys. Rev. B* **78**, 054103 (2008).

[23] L. Chao, E. Colla, and M. Weissman, Aging in the relaxor-ferroelectric  $(\text{PbMn}_{1/3}\text{Nb}_{2/3}\text{O}_3)_{0.90}(\text{PbTiO}_3)_{0.10}$ , *Phys. Rev. B* **74**, 014105 (2006).

[24] B. Vugmeister, Polarization dynamics and formation of polar nanoregions in relaxor ferroelectrics, *Phys. Rev. B* **73**, 174117 (2006).

[25] R. Pirc and R. Blinc, Spherical random-bond-random-field model of relaxor ferroelectrics, *Phys. Rev. B* **60**, 471 (1999).

[26] A. Bray and M. Moore, Metastable states in spin glasses, *J. Phys. C: Solid St. Phys.* **13**, L469 (1980).

[27] B. Drossel and M. Moore, Energy barriers in spin-glasses, *Phys. Rev. B* **70**, 064412 (2004).

[28] V. Westphal, W. Kleeman, and M. Glinchuk, Diffuse phase transitions and random-field-induced domain states of the “relaxor” ferroelectric  $\text{PbMg}_{1/3}\text{Nb}_{2/3}\text{O}_3$ , *Phys. Rev. Lett.* **68**, 847 (1992).

[29] C. Stock, R. Birgeneau, S. Wakimoto, J. Gardener, W. Chen, Z.-G. Ye, and G. Shirane, Universal static and dynamic properties of the structural transition in  $\text{PbZn}_{1/3}\text{Nb}_{2/3}\text{O}_3$ , *Phys. Rev. B* **69**, 094104 (2004).